# On-Chip Detector Cooling for Space Applications

**J.H. Derking[1], H.J.M. ter Brake[1], A. Sirbi[2], M. Linder[2] and H. Rogalla[1]**

[1]University of Twente, Faculty of Science and Technology,
7500 AE Enschede, The Netherlands
[2]European Space Agency, ESTEC
2200 AG Noordwijk, The Netherlands

## ABSTRACT

Vibration-free miniature Joule-Thomson (JT) coolers are of interest for cooling small optical detectors for future space missions. The European Space Agency is interested in on-chip detector cooling for the temperature range 70 K - 250 K. This is the topic of a new project at the University of Twente. In this project, the focus is on the integration of Micro-Electro-Mechanical Systems (MEMS) based JT coolers with small detectors for space applications. Furthermore, distributed micro cooling will be investigated, which means that multiple cold tips will be driven by a single compressor. The progress of this project is discussed in this paper.

The application of JT coolers in the temperature range 70 K - 250 K is investigated. The working fluid in a JT cold stage is optimized on basis of the thermodynamical properties of the fluid. The results of this optimization are discussed. Furthermore, a static model of the counter flow heat exchanger is built, in order to simulate the performance of a micro JT cold stage. The results of the simulations are compared with experimental data.

## INTRODUCTION

Miniature Joule-Thomson (JT) coolers have a high potential for cooling small optical detectors for future earth observation and science missions.[1-3] Both, cooler and detector can be integrated on a single chip by means of Micro-Electro-Mechanical Systems (MEMS) technology.[4] One of the advantages of JT cooling is that a number of cold tips can be driven by a single compressor. In this way, multiple cold tips can be distributed over the satellite, remote from the compressor. This allows for maximum flexibility in satellite design. Another advantage is that by using a sorption compressor, the complete JT cooling cycle is closed without containing moving parts.[5,6] Such a cycle is virtually vibration free and has the potential of a long life time.

Within the Cooling & Instrumentation group at the University of Twente, miniaturization of JT coolers has been a topic of research for more than a decade. Lerou et al.[7,8] have fabricated and tested JT cold stages with a net cooling power around 10 mW. The cold stages were completely made out of D263T glass by means of MEMS-technology. Nitrogen was used as the working fluid at a high pressure of 80 bar and a low pressure of 6 bar. At that low pressure, the boiling point of nitrogen is 97 K. For these cold stages a configuration of the counterflow heat

*Cryocoolers 15*, edited by S.D. Miller and R.G. Ross, Jr.

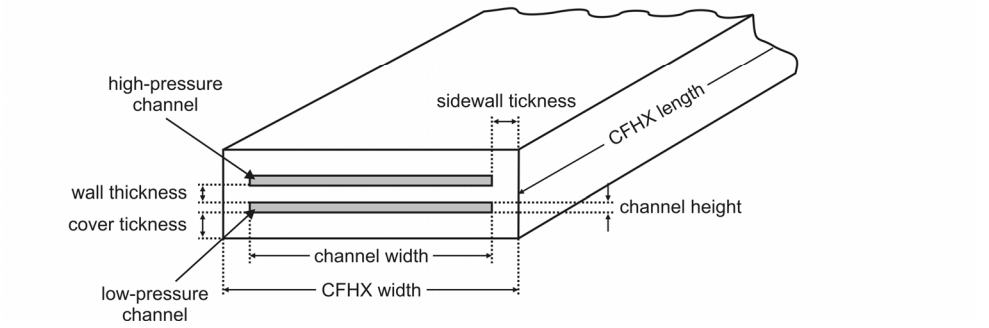


**Figure 1.** Schematic representation of the CFHX of a micro JT cold stage.

exchanger (CFHX) was chosen, where the high-pressure and low-pressure channels were placed on top of one another (see Fig. 1). In the pressure channels, pillars were placed to withstand the high pressures. The dimensions of the cold stage were optimized on the basis of entropy production.[8,9]

The European Space Agency (ESA) is interested in on-chip detector cooling for the temperature range 70 K - 250 K. In the current project at the University of Twente, the aim is to integrate MEMS-based JT cold stages with small optical detectors suitable for use in future space missions. Furthermore, multiple cold tips, operating at different temperatures, will be connected to a single compressor to obtain distributed micro cooling. The progress of this project is discussed in this paper.

## OPTIMIZATION OF THE WORKING FLUID IN A JT COLD STAGE

In order to cover the wide temperature range of 70 K - 250 K by means of JT cooling, different working fluids have to be used. For a JT cold stage operating at a specific temperature, often multiple working fluids can be used. The best working fluid must be selected on the basis of the thermodynamical properties of the fluid. The result of the optimization of the working fluid is described in this section. A more detailed discussion is given by Derking, et al.[10] All fluid properties used in the optimization are taken from Gaspak.[11] Additional thermal conductivity data are taken from Allprops[12] and Promix.[13]

### Selection of the working fluids

The cold-tip temperature of a JT cold stage is determined by the evaporation temperature of the working fluid at the low pressure. This temperature can be varied within a limited range by varying the low pressure. The temperature range in which a working fluid can be used, thus depends on the chosen low-pressure range. For pure working fluids, the cold-tip temperature range is determined, and the result is shown in Fig. 2. The minimum temperature is calculated for a low pressure of 0.2 bar, except for the fluids that have a triple point pressure above 0.2 bar. For these fluids, the minimum temperature corresponds to the triple point pressure. The maximum temperature is calculated for a pressure of 10 bar.

In the figure, it is shown that, for most cold-tip temperatures, multiple working fluids can be used. The best working fluid is selected on the basis of the coefficient of performance of the cold stage (*COP*), which is defined as the ratio of the gross cooling power of the cold stage and the change in Gibbs free energy of the gas during compression. For isothermal compression at a temperature $T_h$, this *COP* can be expressed by

$$COP = \frac{-\Delta h_{comp}}{\Delta h_{comp} - T_h \Delta s_{comp}} \quad . \tag{1}$$

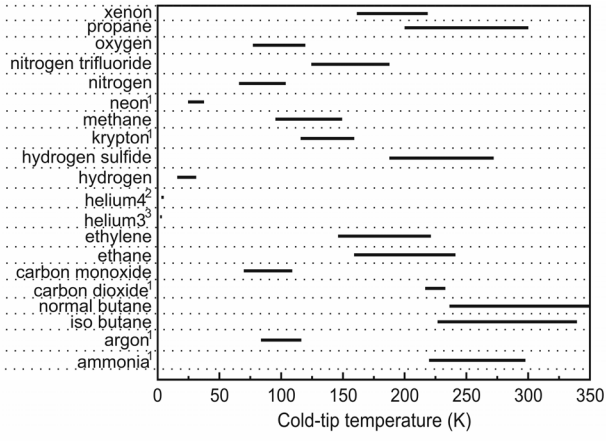


[1] Triple point pressure is used to calculate the minimum temperature.
[2] Minimum temperature corresponds to 0.24 bar and maximum temperature to 1.95 bar.
[3] Minimum temperature corresponds to 0.20 bar and maximum temperature to 1.15 bar.

**Figure 2.** Cold-tip temperature range in which a fluid can be used in a JT cold stage corresponding to a low pressure range of 0.2 - 10 bar.

Here, $\Delta h_{comp}$ is the change in specific enthalpy, and $\Delta s_{comp}$ is the change in specific entropy of the gas during compression.

In addition, a figure of merit (*FOM*) is evaluated, which gives a measure for the effectiveness of the heat exchange in the CFHX. The derivation of this *FOM* is described in more detail elsewhere[10]. The *FOM* is related to the so-called number of heat transfer units (NTU), which is a non-dimensional expression of the 'heat transfer size' of the CFHX[14]. The *FOM* depends on the specific heat ($c_{p,g}$) and the thermal conductivity ($\lambda_g$) of the working fluid and can be written as

$$FOM = \frac{-\Delta h_{comp}}{T_h - T_l} \int_{T_l}^{T_h} \frac{\lambda_g(p,T)}{c_{p,g}(p,T)} dT \,. \tag{2}$$

Here, $T_h$ and $T_l$ are the temperatures of the warm and cold ends of the CFHX, respectively. Except for a geometry factor, the reciprocal value $FOM^{-1}$ gives directly the length needed for the CFHX in order to realize a certain cooling power. The larger the *FOM*, the more efficient is the heat exchange in the CFHX, and thus the shorter the CFHX can be.

## Results

In order to optimize the working fluid in a JT cold stage for different operating temperatures, the *COP* and *FOM* are used. In the optimization, it is assumed that the JT cold stage has a starting temperature of 300 K, that the CFHX is ideal, and that the cooling power is 100 mW. The latter two assumptions are not critical. The fact that the CFHX, in practice, is not ideal, does not play a role in the optimization of the working fluid. The *COP* yields the maximum attainable efficiency and the *FOM* indicates the length of the CFHX that at least is required to achieve that efficiency. Also, the chosen cooling power does not play a part in the optimization of the working fluid. Eq. (1) shows that the *COP* is independent of the mass-flow rate and thus of the required cooling power. Furthermore, the *FOM* is fully determined by the fluid properties and by boundary conditions on temperature and pressure.

For different operating temperatures, the *COP* is calculated as a function of the high pressure. Then, the *FOM* is determined for the optimum high pressure, defined as the pressure for which the *COP* is largest. The maximum *COP* and *FOM* as a function of the cold-tip temperature are given in Fig. 3. In this figure, it is shown that the maximum *COP* increases for

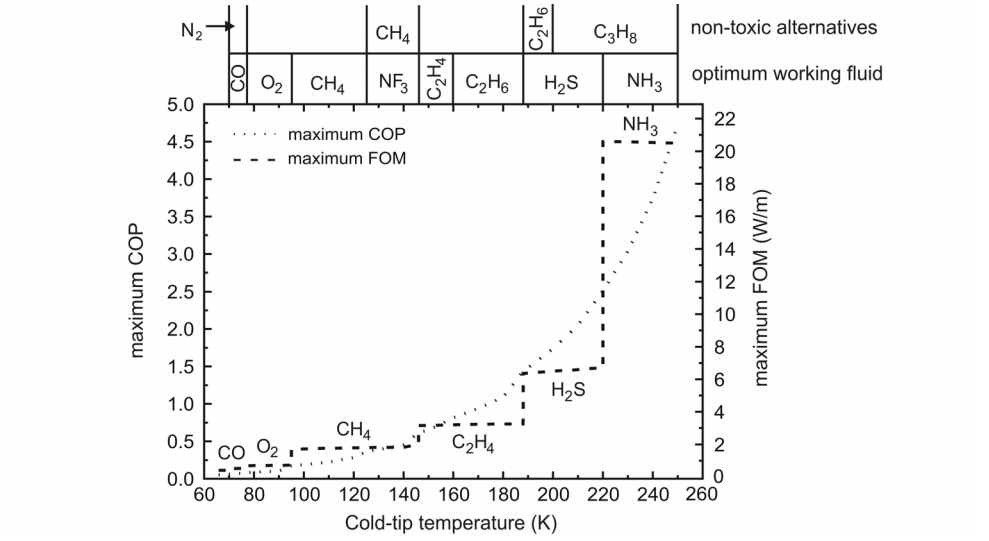


**Figure 3.** Maximum *COP* and *FOM* as a function of the cold-tip temperature and optimum working fluids for a JT cold stage in the temperature range 70 K - 250 K.

an increasing cold-tip temperature. The *FOM* also increases, but some levels of almost constant *FOM* within a small temperature range can be distinguished. Within these small ranges, the *FOM* is determined by a single working fluid. The ratio of specific heat and thermal conductivity is rather constant within that temperature range. This leads to a constant *FOM* (Eq. (2)).

The optimum working fluid is selected on the basis of the *COP*. In the case that the *COP* is almost equal for different working fluids, the *FOM* is evaluated. In this way, the best working fluid is selected for each cold-tip temperature within the wide range of 70 K - 250 K. The optimum working fluid as a function of the cold-tip temperature is also shown in Fig. 3. Some of the fluids that are selected as optimum working fluids are very toxic.[15] Therefore, optimum non-toxic alternatives for these fluids are also given in the figure.

In order to investigate the influence of the starting temperature on the selection of the working fluid, the *COP* and *FOM* are calculated as a function of this temperature. This is done

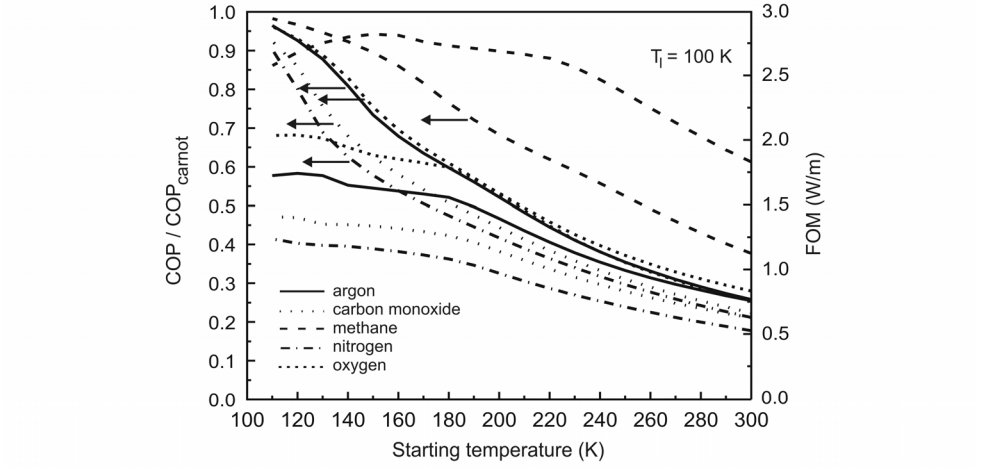


**Figure 4.** *COP* and *FOM* as a function of the starting temperature for a JT cold stage operating at 100 K.

for different cold-tip temperatures. In Fig. 4, a typical example of the *COP* and *FOM* as a function of the starting temperature is shown. To facilitate a better comparison between the different curves, the *COP* is normalized to the Carnot efficiency ($COP_{carnot} = T_l/(T_h-T_l)$). In this example, the operating temperature of the cold stage is 100 K. It is shown that, as expected, the *COP* increases for a decreasing starting temperature. In general, also the *FOM* increases for decreasing starting temperature. Furthermore, it can be concluded that the selection of the optimum working fluid is not affected by the starting temperature.

## SIMULATIONS

In order to simulate the performance of a JT cold stage, integrated with a detector in different thermal environments, a Thermal Mathematical Model (TMM) is built in the software program ESATAN.[16] ESATAN is a program for obtaining solutions to lumped parameter thermal models. In a lumped-parameter model, a continuous medium is modeled as a discrete network of nodes representing the capacitance of the system, linked by conductors representing its conductance. ESATAN has facilities for dealing with conductive, convective and radiative heat transfer. Also, enthalpy flows due to the flow of a fluid through a pipe, can be thermally modeled.

### Static model of the CFHX

For the CFHX of the JT cold stage a configuration is chosen where the high- and low-pressure channels are located on top of one another (see Fig. 1). To simulate the CFHX, the approach of Lerou et al. is used.[8,9] The CFHX is divided into N elements and each element consists of three sub-elements: a high-pressure, a low-pressure, and a material sub-element. The material can be taken as a single element, because the top part, inner wall and bottom part are connected to each other by sidewalls and pillars that are placed in the pressure channels. In the model, longitudinal heat conduction through the CFHX material, as well as radiation on the outer surface of the CFHX, are taken into account. All fluid properties are dependent on temperature and pressure (taken from Gaspak v3.20[11]), and the material properties depend on temperature (taken from Cryocomp v3.01[17]).

A schematic representation of the TMM is given in Fig. 5. As shown, each sub-element is represented by a node. Depending on the type of heat transfer between the nodes, they are

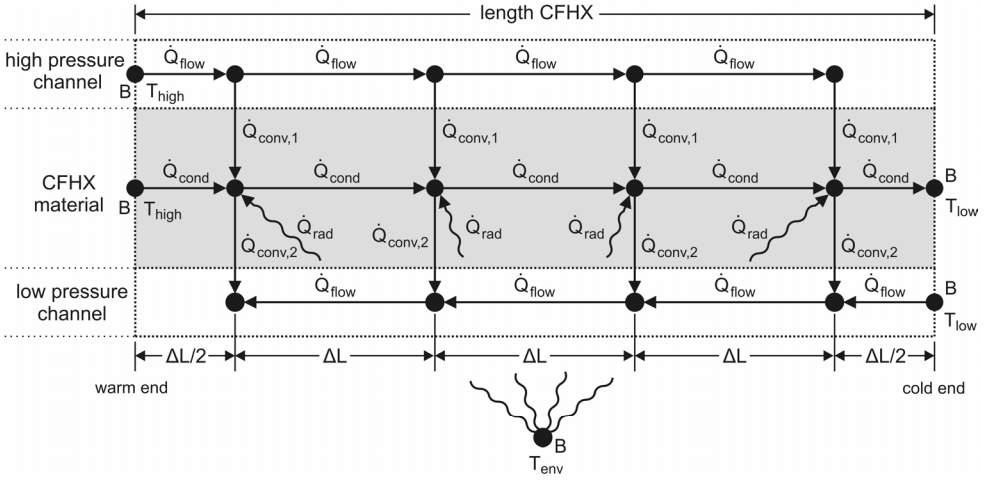


**Figure 5.** Schematic of the TMM in ESATAN. The boundary nodes are indicated by the letter B and the corresponding temperatures are fixed. The radiative conductors, connecting the node of the environment to the CFHX material nodes, are interrupted to obtain a clearer picture.

connected by a conductive, a convective, a radiative, or an enthalpy flow conductor. The various heat flows used in the model are discussed below.

**Enthalpy flow through the CFHX channels.** In the pressure channels, the enthalpy flow is due to the flow of a fluid in the channel. The net heat flow into node i from an upstream node u at temperature $T_u$ can be calculated by

$$\dot{Q}_{flow} = G_F(T_u - T_i) = \dot{m}c_{p,g}(T_u - T_i), \tag{3}$$

where $\dot{m}$ is the mass-flow rate in the channel and $T_i$ is the temperature of node i.

**Convection.** The heat exchange between the high- and low-pressure fluid and the CFHX material takes place via convection and is therefore modeled by a convective conductor. The convective heat flow from a high-pressure node at a temperature $T_{Ph}$ to a material node at a temperature $T_{mat}$ can be written as

$$\dot{Q}_{conv,1} = h_1 A_{hx,1}(T_{Ph} - T_{mat}). \tag{4}$$

Here, $h_1$ is the local heat transfer coefficient and $A_{hx,1}$ is the heat exchange area. The local heat transfer coefficient ($h$) can be defined as $h = \lambda_g Nu/D_h$[18], where $Nu$ is the Nusselt number and $D_h$ is the hydraulic diameter of the channel. At the same way, the convective heat transfer from the material to the low-pressure channel can be expressed by

$$\dot{Q}_{conv,2} = h_2 A_{hx,2}(T_{mat} - T_{Pl}). \tag{5}$$

Because of the configuration chosen for the CFHX, the heat exchange area is equal for both convective heat flows ($A_{hx,1} = A_{hx,2}$).

**Longitudinal conduction through the body of the CFHX.** The longitudinal heat flow through the CFHX material is modeled by connecting the nodes in the material by conductive links. The heat flow between two material nodes at a temperature $T_n$ and $T_m$, respectively, can be calculated by

$$\dot{Q}_{cond} = G_L(T_n - T_m) = \frac{\lambda_{mat} A_{c,mat}}{\Delta L}(T_n - T_m), \tag{6}$$

where $\lambda_{mat}$ is the thermal conductivity of the CFHX material, $A_{c,mat}$ is the total cross-sectional area of the CFHX material, and $\Delta L$ is the distance between the nodes. The longitudinal heat conduction through the fluid is neglected because the longitudinal conduction through the body of the CFHX is much larger.

**Radiation.** The radiation on the outer surface of the CFHX is modeled by radiative conductors connecting the material nodes to the environment. Because in the measurement setup the cold stage is surrounded by a much larger vacuum chamber, the total emissivity of the surroundings is assumed as a black body ($\varepsilon_{sur} = 1$). Also, the surface area of the surroundings is much larger than the surface area of the cold stage. Therefore, the heat flow due to radiation, from an environmental node at a temperature $T_{env}$ to a CFHX material node at a temperature $T_{mat}$, can be written as

$$\dot{Q}_{rad} = \varepsilon_{mat}\sigma_b A_{rad}(T_{env}^4 - T_{mat}^4). \tag{7}$$

Here, $\varepsilon_{mat}$ is the emissivity of the material, $\sigma_b$ is Boltzmann's constant, and $A_{rad}$ is the outer surface area of a node of the CFHX. Because the emissivity of the glass is quite large ($\varepsilon = 0.8$ to 0.95[19]), a thin layer of gold ($\varepsilon = 0.02$[20]) is sputtered on top of the outer surface of the cold stage.

**Boundary conditions on temperature.** In the measurement setup, the environment of the cold stage is assumed to be at a constant temperature and can thus be modeled as a single node at a temperature $T_{env}$. Also, two boundary temperatures can be set. The temperature of the cold end ($T_{low}$) depends on the low pressure and thus is fixed. Therefore, the input node of the low-pressure channel as well as the material node at the cold end will be at this temperature. The temperature at the warm end of the CFHX ($T_{high}$) depends on the chosen starting temperature of the JT cold stage. This means that also the temperature at the input of the high-pressure channel

**Table 1.** Various JT cold-stage designs with calculated and measured cooling powers.

| prototype | **1** | **2** | **3** | **4** | **5** | **6** | **7** |
|---|---|---|---|---|---|---|---|
| length of the cfhx (mm) | 25 | 15 | 35 | 25 | 35 | 25 | 35 |
| width of the cfhx (mm) | 2 | 2 | 2 | 2 | 2 | 4 | 5 |
| mass flow (mg $s^{-1}$) | 1 | 1 | 1 | 2 | 2 | 2 | 3 |
| gross cooling power (mW) | 14.7 | 14.7 | 14.7 | 29.5 | 29.5 | 29.5 | 44.2 |
| $P_{net}$ calculated (mW) | 12.2 | 10.6 | 12.8 | 21.9 | 24.8 | 25.2 | 39.7 |
| $P_{net}$ measured (mW) | 11 ± 2 | 9 ± 2 | xxx | 15.5 ± 2 | 24 ± 2 | 21 ± 2 | xxx |

and that of the material of the CFHX at the warm end need to be fixed. In Fig. 5, the boundary nodes are indicated by the letter B.

**Cooling power.** In this TMM, the net cooling power of the micro JT cold stage can be calculated by the difference in enthalpy of the high-pressure fluid ($H_{Ph,in}$) and the low-pressure fluid ($H_{Pl,out}$) at the warm end of the CFHX minus the total radiative heat flow on the outer surface of the JT cold stage ($\Sigma \dot{Q}_{rad}$)

$$P_{net} = \dot{m}(h_{Ph,in} - h_{Pl,out}) - \sum \dot{Q}_{rad} \ . \tag{8}$$

The total radiative heat flow is the sum of the radiation terms on the CFHX and on the evaporator.

**Results of the simulations**

A static TMM of the CFHX is built in ESATAN. In order to compare the TMM with experimental data, data is used corresponding to measurements performed by Lerou et al.[8] Nitrogen is chosen as the working fluid. The high pressure is taken at 80 bar and the low pressure at 6 bar. This means that the cold-tip temperature is fixed at 97 K. The temperature of the environment and the starting temperature of the cold stage are both taken as 300 K.

Simulations have been performed for different designs of the cold stage. In Table 1, the parameters of the different designs are summarized. In all designs, the height of the channels is 50 μm, the thickness of the top, bottom and sidewalls is 150 μm, and the thickness of the wall between the high- and low-pressure channel is taken as 100 μm. The length and width of the CFHX is changed as well as the mass-flow rate. Also, the gross cooling power and the calculated

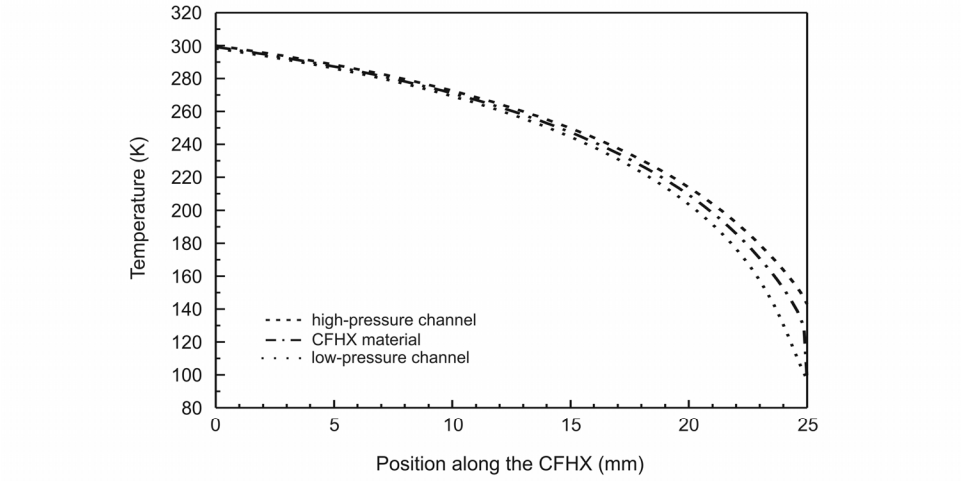


**Figure 6.** Temperature profile of the high-pressure gas, CFHX material and low-pressure gas as a function of the position along the CFHX.

net cooling power are given in the table. In Fig. 6, typical temperature distributions along the high-pressure channel, material and the low-pressure channel are shown as a function of the position along the CFHX.

Lerou et al.[7,8] fabricated and tested the different designs of the cold stage summarized in Table 1. The measured cooling powers are included in the table. These values are already compensated for the parasitic heat load of the measurement setup, which is between 6 mW and 10 mW.[8] From the table it can be concluded that for cold stage 1, 2 and 5, the calculated net cooling power agrees very well with the measured ones. The measured cooling powers of cold stages 4 and 6 are lower than the calculated ones. For cold stage 4, this is probably due to defects in the reflective shield of the cold stage that increases the emissivity, and thus decreases the net cooling power.[8] On cold stage 6, the resistor added to measure the cooling power was not correctly glued to the cold tip. This resulted in a higher surface area, which increases the radiative heat load, and thus decreases the cooling power.[8] It can thus be concluded that the TMM agrees very well with the experimental results.

**TMM of the integrated system**

The goal of the TMM is to simulate the performance of a JT cold stage integrated with a small optical detector in different thermal environments. The first step to reach this goal is to build a dynamic model of the JT cold stage. This can be done by connecting the evaporator to the CFHX. Such a dynamic model can be used to simulate the performance of a JT cold stage in time and to calculate the cooldown time of the system. The next step is to build a model of a detector and integrate both models by defining thermal conductors between them. Cabling of the detector also has to be taken into account. In this way, a TMM of the integrated system will be built and used to simulate the performance of a MEMS-based JT cold stage integrated with an optical detector.

## CONCLUSIONS

JT micro cooling is an ongoing topic of research at the Cooling & Instrumentation group of the University of Twente. In the current project the focus is on the integration of MEMS-based JT cold stages with small optical detectors for space applications. Furthermore, distributed micro cooling will be investigated.

In the temperature range 70 K - 250 K, the working fluid in a JT cold stage is optimized on the basis of the *COP*, which is defined as the gross cooling power divided by the change in Gibbs free energy during compression. In addition, a *FOM* is evaluated, which depends on the specific heat and thermal conductivity of the working fluid. The FOM gives a measure for the effectiveness of the heat exchange in the CFHX. The optimum working fluid is determined depending on the cold-tip temperature within the range of 70 K - 250 K. The non-toxic ones for a specific temperature range (within brackets) are nitrogen (70-77 K), oxygen (77-95 K), methane (95-146 K), ethylene (146-160 K), ethane (160-200 K) and propane (200-250 K). It is shown, that decreasing the starting temperature does not have an influence on the selection of the optimum working fluid.

A static model of the CFHX has been built in the software program ESATAN. With this model, the temperature profile of the high- and low- pressure channel and the material along the length of the CFHX can be determined as well as the net cooling power. For five different designs of the CFHX, the net cooling power has been calculated and compared with experimental data. Two of these had defects in the experimental setup, resulting in a cooling power lower than calculated. The remaining three designs showed calculated net cooling powers within the margins of the measured ones. For example, for one of the designs, the measured net cooling power is 11±2 mW and the calculated one 12.2 mW. The static model of the CFHX can thus be used to predict the performance of a JT cold stage.

**ACKNOWLEDGMENT**

This work was supported by the European Space Agency under Contract No. 20678.

**REFERENCES**

1. Bhandari, P., Prina, M., Bowman Jr, R.C., Paine, C., Pearson, D., Nash, A., "Sorption coolers using a continuous cycle to produce 20 K for the Planck flight mission," *Cryogenics*, vol. 44 (2004), pp. 395-401.
2. Burger, J.F., ter Brake, H.J.M., Rogalla, H., Linder, M., "Vibration-free 5 K sorption coolers for ESA's Darwin mission," *Cryogenics*, vol. 42 (2002), pp. 97-108.
3. Levenduski, R., Scarlotti, R., "Joule-Thomson cryocooler for space applications," *Cryogenics*, vol. 36 (1996), pp. 859-866.
4. Elwenspoek, M., Jansen, H., *Silicon micromachining*, Cambridge University Press, Cambridge (1998).
5. Wiegerinck, G.F.M., Burger, J.F., Holland, H.J., Hondebrink, E., ter Brake, H.J.M., Rogalla, H., "A sorption compressor with a single sorber bed for use with a Linde-Hampson cold stage," *Cryogenics*, vol. 46 (2006), pp. 9-20.
6. Wiegerinck, G.F.M., *Improving sorption compressors for cryogenic cooling*, Ph.D. Thesis, University of Twente, Enschede, The Netherlands (2005).
7. Lerou, P.P.P.M., Venhorst, G.C.F., Berends, C.F., Veenstra, T.T., Blom, M., Burger, J.F., ter Brake, H.J.M., Rogalla, H., "Fabrication of a micro cryogenic cold stage using MEMS-technology," *J. Micromech. Microeng.*, vol. 16 (2006), pp. 1919-1925.
8. Lerou, P.P.P.M., *Micromachined Joule-Thomson Cryocooler,* Ph.D. Thesis, University of Twente, Enschede, The Netherlands (2007).
9. Lerou, P.P.P.M., Veenstra, T.T., Burger, J.F., ter Brake, H.J.M., Rogalla, H., "Optimization of counterflow heat exchanger geometry through minimization of entropy generation," *Cryogenics*, vol. 45 (2005), pp. 659-669.
10. Derking, J.H., ter Brake, H.J.M., Sirbi, A., Linder, M., Rogalla, H., "Optimization of the working fluid in a Joule-Thomson cold stage," submitted for publication to Cryogenics.
11. Arp, V., McCarthy, R.D., Fox, J.R., *Gaspak v. 3.20*, Horizon Technologies, available online on http://www.htess.com/gaspak.htm
12. Allprops v 4.2, The center of thermodynamics studies, University of Idaho, Idaho (1996).
13. Ely, J.F. et al., Promix version 1.02b, Horizon Technologies.
14. Kays, W.M., London, A.L., *Compact heat exchangers*, 3rd ed., McGraw-Hill Book Co (1984).
15. Air Liquide, *encyclopedia*, <http://encyclopedia.airliquide.com>.
16. ESATAN™ 10.0, Alstom Energy Technology Centre (2006).
17. Cryocomp v 3.01, Cryodata Inc, Eckels engineering, Florence SC, USA.
18. Bejan, A., *Heat transfer*, John Wiley and Sons Inc (1993).
19. Hsieh C.K., Su, K.C., "Thermal radiative properties of glass from 0.32 to 206 μm," *Solar Energy*, vol. 22 (1979), pp. 37-43.
20. Bendavida, A., Martina, P.J., Wieczorekb, L., "Morphology and optical properties of gold thin films prepared by filtered arc deposition," *Thin Solid Films*, vol. 354 (1999), pp. 169-175.